Power-law banded random matrix ensemble as a model for quantum many-body Hamiltonians

Wouter Buijsman,[1,*] Masudul Haque,[2,1,†] and Ivan M. Khaymovich[3,‡]

[1] *Max Planck Institute for the Physics of Complex Systems, 01187 Dresden, Germany*
[2] *Institut für Theoretische Physik, Technische Universität Dresden, 01062 Dresden, Germany*
[3] *Nordita, Stockholm University & KTH Royal Institute of Technology, SE-106 91 Stockholm, Sweden*

(Dated: March 12, 2025)

Hamiltonians of one-dimensional, disordered single-particle systems with long-range hopping terms can naturally be modeled by power-law banded random matrices. In this picture, the phase diagram of the power-law banded random matrix ensemble show ergodic, weakly ergodic, multifractal, and localized phases. Motivated by recent developments on ergodicity breaking and localization in interacting quantum many-body systems, we explore many-body interpretations of the power-law banded random matrix ensemble. We discuss a number of ways to label the basis vectors with many-body configurations, and compare the physical properties of the resulting Hamiltonians. We characterize the scaling of the many-body eigenstate entanglement entropy with system size for the different labeling schemes and in each of the phases. Using a scaling analysis on the full sets of eigenstates, we subsequently provide a quantitative picture of the boundary between the different types of scaling behavior that we observe for the spectral-bulk and spectral-edge eigenstates.

I. INTRODUCTION

Disordered quantum many-body systems provide an active topic of research [1], in recent years in particular in the context of (the stability of) many-body localization [2, 3] and quantum computation [4–6]. Much of our understanding of disordered quantum systems is rooted in the theory of random matrices [7–9]. Random matrix models can provide simplified phenomenological descriptions of complicated disordered quantum systems, without loosing the main physical features. In addition, random matrix ideas are central to our current understanding of thermalization of isolated quantum systems and quantum many-body chaos, with or without disorder [10–20].

The most prominent random matrix ensembles used to model quantum Hamiltonians are the Gaussian orthogonal (GOE) and unitary (GUE) ensembles, for which the matrix elements are identically distributed. In many physical situations, remote basis states are on average less strongly coupled than nearby basis states. Examples of random matrix models which incorporate this idea or its variants, studied recently in the context of ergodicity breaking, include the Rosenzweig-Porter model [21–27] and recently proposed variations thereof [28–37], ultrametric random matrix models [38–46], and power-law banded random matrix models [39, 40, 42, 44, 47–56]. The last is the focus of the present work.

Power-law banded random matrices have uncorrelated (up to Hermiticity) normally distributed elements with mean zero and a variance that decays in a power-law fashion as a function of the distance from the main diagonal [44, 47, 49, 51]. Determined by the power law exponent, the eigenvectors can either be (fully or weakly) ergodic, multifractal, or localized. Interpreting power-law banded random matrices as Hamiltonians of one-dimensional single-particle quantum systems has proven to be a meaningful exercise in studying Anderson localization [50, 52, 57–59]. Recently, generalized forms of power-law banded random matrices gained interest in studying ergodicity breaking in non-Hermitian [60–62] and periodically driven [63] systems.

Motivated by recent theoretical, computational, and experimental developments on ergodicity breaking and localization in interacting quantum many-body systems, in this work we explore many-body interpretations of the power-law banded random matrix ensemble. The usual random-matrix description of many-body Hamiltonians with matrix classes GOE or GUE has the shortcoming that the eigenvectors of such random matrices have similar properties in the spectral bulk and at the spectral edges. In contrast, for physical many-body Hamiltonians, the low-energy eigenstates have markedly different entanglement properties compared to the eigenstates in the spectral bulk [64]. Power-law banded random matrices reflect this distinction between edge and bulk eigenstates, as noted in Ref. [56]. Thus, the power-law banded random matrix ensemble provide an improved model of the structure of chaotic many-body Hamiltonians. In addition, many-body interpretations of the power-law banded random matrix ensemble are of potential interest in studies of localization (or the lack thereof) in disordered interacting quantum many-body systems [65].

When interpreting GOE or GUE matrices as physical Hamiltonians, the basis labels can be assigned arbitrarily to the physical basis states, since these matrices have no structure. For interpreting structured random matrices as Hamiltonians of quantum many-body systems, assigning a physical interpretation to the basis vectors is a trickier issue. One wants to do this in such a way

* buijsman@pks.mpg.de
† masudul.haque@tu-dresden.de
‡ ivan.khaymovich@gmail.com

that the resulting Hamiltonian resembles or models a system with only few-body, short-range interactions. In Refs. [56, 65], each basis vector is assigned a (different) many-body product state, where the index is obtained by interpreting it as a binary number of L bits, where L is the number of lattice sites.

In the present work, we provide a more systematic study of interpreting power-law banded random matrices as Hamiltonians of quantum many-body systems. After a brief review of power-law banded random matrices (Sec. II), we first identify three different ways to label basis vectors with many-body configurations (Sec. III). We quantify the quality of the labeling schemes, and argue one of our labeling schemes to improve on the one proposed previously. We discuss how to resolve an issue regarding the homogeneity of the resulting Hamiltonians using what we will refer to as "site randomization". Second (Sec. IV), we investigate physical properties of the resulting Hamiltonians. We study the scaling of the eigenstate entanglement entropy with system size in the different phases of the model. By studying the finite-size effects (Sec. V), we estimate the value of the power-law exponent separating area-law from volume-law scaling, which we find to be different for eigenstates at the bulk and the edge of the energy spectra. Additionally (Sec. VI), using a scaling analysis on the full sets of eigenstates, we provide a quantitative picture of the boundary between the different types of scaling behavior for spectral-bulk and edge eigenstates. We conclude (Sec. VII) with a brief summary and some open questions left for future investigations.

II. POWER-LAW BANDED RANDOM MATRICES

Various related definitions of the power-law banded random matrix ensemble are in use in the literature [52]. Matrices H sampled from such an ensemble are typically element-wise defined as

$$H_{ij} = G_{ij}\, a(|i-j|), \tag{1}$$

where $G_{ij} = G_{ji}$ are independent and identically distributed random numbers, representing the Gaussian orthogonal (GOE) random matrix ensemble. The GOE consists of real-valued symmetric matrices with entries sampled independently from the Gaussian distribution with mean $\mu = 0$ and off-diagonal (diagonal) components with variance $\sigma^2 = 1/2$ ($\sigma^2 = 1$) [7]. Next, the function $a(r)$ decays as a power law for $r \gg 1$, with a tunable coefficient $\alpha > 0$. Here, we take

$$a(r) = \frac{1}{1 + (r/\beta)^\alpha} \tag{2}$$

with the so-called bandwidth β set to unity ($\beta = 1$). This definition has been part of investigations previously in Ref. [56], involving some of the present authors.

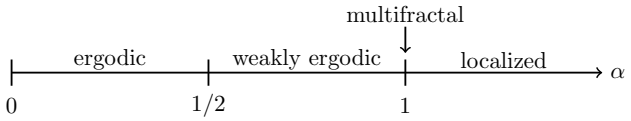

FIG. 1. The phase diagram of the power-law banded random matrix ensemble, showing the phases of mid-spectrum eigenstates as a function of the power-law exponent α. See the main text for details.

Other often used definitions can be found, for example, in Refs. [44, 47, 49].

In the single-particle interpretation, the parameter α allows one to tune the eigenstates in the bulk (middle) of the spectrum in a fully ergodic ($\alpha < 1/2$) [43], weakly ergodic ($1/2 < \alpha < 1$) [44], or (power-law) localized ($\alpha > 1$) phase [47]. In the fully ergodic phase, the properties of the model are statistically the same as those of the GOE. This means that for an eigenstate $|\psi\rangle$, the inverse participation ratio $\sum_n |\langle n|\psi\rangle|^4$ with the summation running over all basis states $|n\rangle$ ($n = 1, 2, \ldots, N$) is asymptotically given by $3/N$. The weakly ergodic phase is characterized by bulk eigenstates occupying only a finite fraction of the Hilbert space [44, 66]. Here, the inverse participation ratio of the eigenstates is asymptotically given by c/N for some $c > 3$ depending on α. The fractal dimensions D_q ($q \geq 1$) of an eigenstate $|\psi\rangle$ are defined through the scaling

$$\sum_n |\langle n|\psi\rangle|^{2q} \sim N^{-D_q(q-1)}. \tag{3}$$

The ergodic and weakly ergodic phases are characterized by eigenstates with unit fractal dimensions ($D_q = 1$). At the critical point $\alpha = 1$, the eigenstates in the bulk of the spectrum are multifractal ($0 < D_q < 1$ is a q-dependent function), and level statistics are intermediate between Poisson and Wigner-Dyson. In the localized phase, the eigenstates have fractal dimension zero for positive integers q, meaning that the inverse participation ratio does not scale with N and the eigenstates only occupy a measure zero of the full Hilbert space. Fig. 1 provides a graphical summary of the phase diagram discussed here.

The phenomenology of power-law banded random matrices can be understood from resonance counting [67, 68] and the Breit-Wigner approximation (see, for example, Refs. [27, 69]). First, from the resonance counting arguments, it follows that localization perturbation theory converges if the number $N_{\rm res}$ of resonances, defined as $|H_{mn}| > |H_{nn} - H_{mm}|$, does not grow with the size N of the matrix [29, 31, 54]. To calculate $N_{\rm res}$, one should sum the probabilities of the other nodes $m \neq n$ to be in resonance with node n. For identically, independently uniformly distributed diagonal elements $|H_{ii}| < W/2$, one obtains

$$N_{\rm res} = \sum_{\substack{m=1 \\ m\neq n}}^{N} \int_{-W}^{W} P(H_{mn}) |H_{mn}| dH_{mn}. \tag{4}$$

In the case of normal distribution of H_{ii} the above expression is the same in the leading order up to an unimportant prefactor. For power-law banded random matrices the above integral gives $\int_{-W}^{W} P(H_{mn})|H_{mn}|dH_{mn} \sim R^{-\alpha}$ and leads to $N_{\rm res} \simeq \sum_{R=1}^{N} R^{-\alpha} \sim N^{1-\alpha} + \mathcal{O}(1)$, which converges for $\alpha > 1$. Therefore, for $\alpha > 1$ one expects localized eigenstates.

Second, the Breit-Wigner approximation is based on Fermi's golden rule where the level broadening

$$\Gamma_n(E) = \frac{2\pi}{\hbar}\nu(E) \sum_{\substack{m=1 \\ m\neq n}}^{N} |H_{mn}|^2, \tag{5}$$

with the normalized density of states $\nu(E)$, enters the wave-function estimate as

$$|\psi_E(n)|^2 \simeq \frac{A\Gamma_n(E)}{(E-H_{nn})^2 + \Gamma_n(E)^2}, \tag{6}$$

with a certain normalization prefactor A [27, 69]. As soon as $\Gamma(E) \equiv \langle \Gamma_n(E) \rangle \gg \langle H_{nn}^2 \rangle$ for all the energies E, all the wave-function coefficients are of the same order and, therefore, all the states should be ergodic. For power-law banded random matrices, one obtains $\Gamma_n(E) \sim \sum_{R=1}^{N} R^{-2\alpha} \sim N^{1-2\alpha} + \mathcal{O}(1)$. This diverges at $\alpha < 1/2$ for all the energies. Therefore, for $\alpha < 1/2$, one expect all the eigenstates to be ergodic (statistically equivalent to those of the GOE). Together, these two lines of arguments predict the phase diagram shown in Fig. 1.

Regarding the intermediate region $1/2 < \alpha < 1$ in-between the ergodic ($\alpha < 1/2$) and localized ($\alpha > 1$) phases, it has been established that mid-spectrum eigenstates are weakly ergodic, as pointed out above [44, 47]. More recent numerical results suggests that the spectral edge eigenstates behave differently [56, 65]. This difference between edge and bulk eigenstates is a strong reason for considering power-law banded random matrices to be an improved model for many-body Hamiltonians, as compared to non-banded matrices (GOE or GUE) which do not show such a difference. In this paper we will explore the difference between spectral bulk and edge eigenstates in detail.

III. BASIS STATE LABELING

We aim to interpret the power-law banded random matrix ensemble as Hamiltonians of quantum many-body systems. This can be accomplished by associating each basis vector with a (different) many-body configuration. We will focus on spin-1/2 chains in this work. For simplicity, we restrict to systems without any conservation laws. The Hamiltonian of an L-site system is then modeled as a random matrix of dimension $N = 2^L$. Assigning many-body configurations to basis vectors can be done in various ways. Here, we first propose three different labeling schemes, which we refer to as "random", "binary", and "Gray code". The binary labeling scheme has been considered before in Refs. [56, 65]. We propose a way to quantify the quality of a labeling scheme, and find the Gray code scheme to be of higher quality than the binary one. We find the (ensemble-averaged) Hamiltonians for the binary and Gray code labeling schemes to be non-homogeneous, meaning that the physical properties are dependent on the site index. We next discuss how to correct for this through what we will refer to as "site randomization".

The issue of labeling scheme is significant when using banded random matrices as a model for many-body Hamiltonians. This is in contrast to the case of using random matrix models characterized by identically distributed off-diagonal elements (e.g., GOE or GUE). In the latter (more conventional) case, any labeling scheme would lead to the same Hamiltonian on average.

A. Labeling schemes

We represent many-body configurations c_i (for example, $c_i = 001111$) with i ranging over integers from one to N by L binary digits, where the j-th digit is zero (one) if the j-th spin is in the down (up) state. In power-law banded random matrices, the matrix elements between configurations with neighboring labels have larger magnitude on average. Since physical Hamiltonians contain few-body operators, we thus want neighboring configurations to differ from each other by as few spin flips as possible.

In what follows, we quantify the quality of a given labeling scheme by the "badness"

$$B = \frac{1}{N-1} \sum_{i=1}^{N-1} d_2(c_i, c_{i+1}). \tag{7}$$

Here, $d_2(c_i, c_j)$ represents the Hamming distance between the many-body configurations c_i and c_j, i.e., the the minimum number of spin flips connecting the two configurations. Here the subscript 2 indicates that the numbers are represented in binary digits. The badness penalizes for successive many-body configurations c_i and c_{i+1} to be separated by a large number of spin flips.

Arguably the most straightforward way to assign different many-body configurations to basis states is by doing this randomly. Such a labeling scheme can be implemented by randomly ordering all many-body configurations, and assigning each to a basis state. Interactions in the many-body picture of the random labeling scheme are non-local and tend to involve many spins.

In the thermodynamic limit $L \gg 1$, the set of all possible many-body configurations is dominated by configurations with (close to) $L/2$ up-spins. The average Hamming distance between two randomly selected basis states approaches then $L/2$, since one (on average) needs to flip $L/4$ spins from down to up, and $L/4$ spins from up to

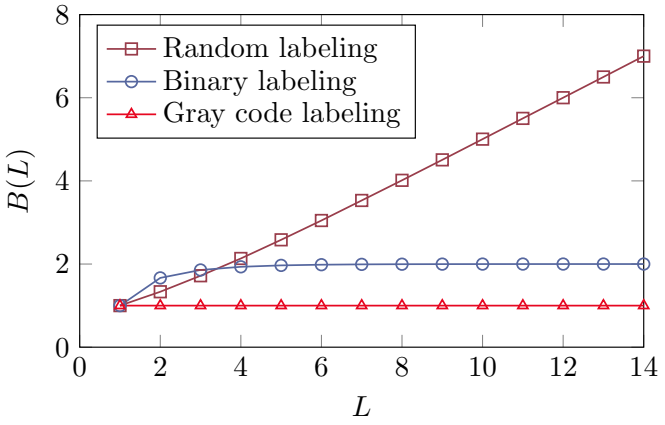

FIG. 2. The badness (7) as a function of the system size L for each of the labeling methods. For the random labeling scheme, the sample-to-sample variance is smaller than the marker size.

down. For the random labeling scheme, one thus has that $B(L) \approx L/2$ for large L (Figure 2).

A lower badness can be achieved by adapting a labeling scheme that prefers the configurations c_i and c_{i+1} to be separated by a smaller number of spin flips. This can be accomplished by taking c_i to be the binary representation of $i-1$. We refer to this as the "binary" labeling scheme; this was used in Ref. [56, 65]. For $L = 3$, as an example, the labels are

$$c_1 = 000 \quad c_2 = 001 \quad c_3 = 010 \quad c_4 = 011$$
$$c_5 = 100 \quad c_6 = 101 \quad c_7 = 110 \quad c_8 = 111.$$

We find numerically (and it can be argued combinatorially) that the badness approaches $B(L) \approx 2$ for $L \gg 1$ for the binary labeling scheme (Figure 2). This is significantly lower than the scaling $B(L) \approx L/2$ for the random labeling scheme.

The Gray code provides an ordering of the binary numbers such that successive numbers differ by only a single element [70, 71]. We refer to the corresponding labeling scheme as the "Gray code" labeling scheme, which is characterized by the lowest possible badness $B(L) = 1$. The configuration c_n in the binary labeling scheme can be converted to the corresponding configuration in the Gray code labeling scheme by taking all up to the first nonzero digit identical. The subsequent digits are equal to 1 if the corresponding and previous digit in the binary representation are different (i.e., 0 and 1), and 0 otherwise. Taking $L = 3$ again as an example, one finds

$$c_1 = 000 \quad c_2 = 001 \quad c_3 = 011 \quad c_4 = 010$$
$$c_5 = 110 \quad c_6 = 111 \quad c_7 = 101 \quad c_8 = 100.$$

We note that there is no unique labeling scheme with the lowest possible badness. One can understand this, for example, by observing that the badness does not change when changing the ordering of the digits. Fig. 2 shows the badness as a function of the system size for the random, binary, and Gray code labeling methods. Clearly, the asymptotic scaling is well-approximated already at small system sizes.

The badness (7) used to quantify the quality of a chosen basis state labeling scheme is rather simple. In principle, it is possible to define more sophisticated probes that are sensitive to other features one might wish a labeling scheme to have. For example, one might want to penalize successive configurations for having pairs of spin flips which are far from each other, and one might want to consider pairs of configurations with labels differing by more than one. For the purposes of the present discussion, the badness as defined in Eq. (7) is sufficient.

B. Site randomization

Despite having a low badness, the binary and Gray code labeling schemes do not lead to physically natural Hamiltonians. For the binary labeling scheme, changing the n-th digit (counted from the right and starting at zero) from zero to one in the binary representation increases the index that is represented by 2^n. For Hamiltonians given by power-law banded random matrices, such a hierarchy between basis states means that interactions between spins are weaker for sites on the left than for sites on the right. Aiming to illustrate the physical consequences, we here numerically study the entanglement entropy of mid-spectrum eigenstates for the binary labeling scheme at the transition point between the weakly ergodic and localized phase ($\alpha = 1$). The entanglement entropy of fully ergodic (structureless) eigenstates for a decomposition in subsystems A (size L_A) and B (size L_B) is well-approximated by the Page value [72, 73]

$$S_{\text{Page}} = \ln(2)\, \min(L_A, L_B) - \frac{2^{\min(L_A,L_B)}}{2^{\max(L_A,L_B)+1}}\,. \qquad (8)$$

Here, subsystems A and B cover the leftmost L_A and rightmost $L_B = L - L_A$ sites, respectively. Fig. 3 shows the ensemble-averaged eigenstate entanglement entropy S_{ent} of mid-spectrum eigenstates as a function of the subsystem fraction L/L_A for various total system sizes, together with reference values (8).

For $L_A/L \approx 1$, the eigenstate entanglement entropy is close to the Page value (dotted line). The entropy is much smaller than the Page value for $L_A/L \approx 0$. In order to understand this asymmetry, we start by noting that multifractal eigenstates essentially have overlap only with a vanishing fraction of the basis states [15]. Due to this, such basis states tend to have the same binary digits near the left edge (covering subsystem A), while they tend to have different binary digits near the right edge (covering subsystem B). When the cut between the subsystems is near the left edge (L_A is small), measurements of the state of the left subsystem typically give the same result, while measurements of the state of the right subsystem typically gives different results. This leads to

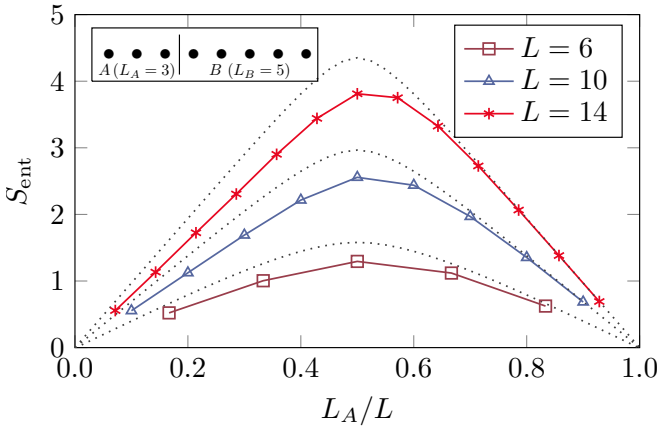

FIG. 3. The ensemble-averaged eigenstate entanglement entropy for mid-spectrum eigenstates for power-law banded random matrices with $\alpha = 1$ computed using the binary labeling scheme (no site randomization). The spin chain is decomposed in subsystems A and B consisting of the first L_A and last $L_B = L - L_A$ sites, respectively. The inset illustrates the decomposition for $L_A = 3$ and $L_B = 5$. The dotted lines give the Page values (8) for the system sizes and decompositions under consideration.

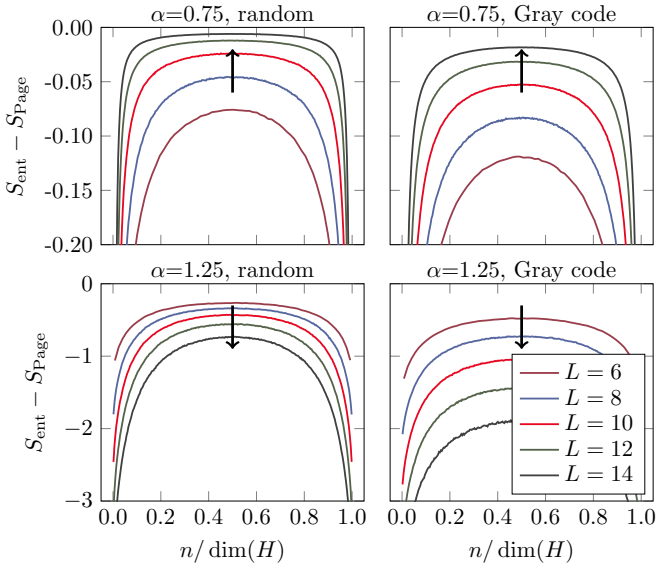

FIG. 4. The difference between the ensemble-averaged eigenstate entanglement entropy and the Page value as a function of the eigenstate index n (starting from $n = 1$ and ordered by increasing energy), scaled by $\dim(H)$ for the random and Gray code labeling schemes at $\alpha = 0.75$ and $\alpha = 1.25$. The arrows indicate the direction of flow with increasing system size. Note the vastly different scales on the vertical axes for the upper and lower panels.

non-symmetric curves when plotting the eigenstate entanglement entropy as a function of L_A or L_A/L.

In what follows, we randomize the L real-space site indices, corresponding to the binary digits of the many-body configurations, in order to avoid the (ensemble-averaged) Hamiltonians to be non-homogeneous. We refer to this procedure as "site randomization". For the ensemble-averaged results shown below, both the Hamiltonian and the site ordering have been sampled independently for each realization.

IV. ENTANGLEMENT OF EIGENSTATES

We now analyze the many-body interpretations of the power-law banded random matrix ensemble introduced above. Our focus is on the ensemble-averaged eigenstate entanglement entropy for a bipartition of the system in left and right halves of equal size ($L_A = L_B = L/2$). Fig. 4 illustrates its dependence on the power-law exponent α, the basis state labeling scheme, the system size, and the location on the energy spectrum. It shows the rainbow-like structure, mentioned in [56] with larger entanglement in the bulk and smaller at the spectral edges.

Regarding the eigenstates associated with eigenvalues in the bulk (middle part) of the spectrum, we can make a number of observations: (i) in the weakly ergodic phase (upper panels), $S_{\rm ent}$ gets closer to $S_{\rm Page}$ with increasing system size; (ii) in the localized phase (lower panels) $S_{\rm ent}$ deviates away from $S_{\rm Page}$ with increasing system size; (iii) in both the weakly ergodic and localized phases, adapting the random labeling scheme (left panels) leads to values of $S_{\rm ent}$, closer to $S_{\rm Page}$ than adapting the Gray code labeling scheme (right panels). Regarding the eigenstates associated with eigenvalues near the edges of the spectrum, we observe that $S_{\rm ent}$ strongly deviates from $S_{\rm Page}$ in both the weakly ergodic and the localized phases. Thus, in the next two subsections we focus separately on the spectral bulk and edge states.

A. Spectral bulk eigenstates

Fig. 5 shows the entanglement entropy and the difference from the Page value for mid-spectrum eigenstates as a function of α for the random and Gray code labeling schemes at several system sizes. For $\alpha \lesssim 1$, we observe volume-law ($S_{\rm ent} \sim L$) scaling for both labeling schemes. In fact, the data suggests that $S_{\rm ent} \approx S_{\rm Page}$ in the thermodynamic limit. For $\alpha \gtrsim 1$, we observe area-law scaling ($S_{\rm ent} \sim L^0$), again for both labeling schemes. The random labeling scheme appears to be more sensitive to finite-size effects. The difference $S_{\rm Page} - S_{\rm ent}$ shows an approximate crossing for different system sizes at $\alpha \approx 1$, again for both labeling schemes. In Sec. V, we study this crossing, which marks the transition between volume-law scaling and area-law scaling, quantitatively.

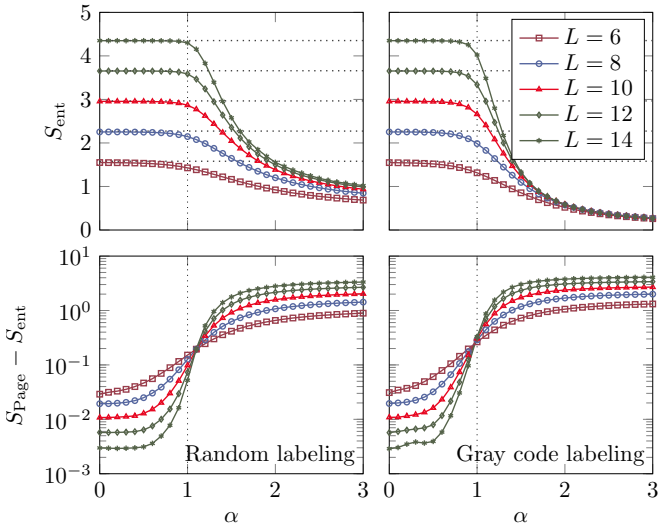

FIG. 5. The ensemble-averaged eigenstate entanglement entropy (upper panels) and the difference with the Page value (lower panels) for mid-spectrum eigenstates as a function of α. The left and right panels show data for the random and Gray code labeling scheme, respectively. The horizontal dashed lines give the Page values for the system sizes under consideration. The vertical dotted lines mark $\alpha = 1$. Here, the eigenstates with indices n (starting from $n = 1$ and ordered by increasing energy) ranging from $\dim(H)/2-10$ to $\dim(H)/2+10$ are analyzed.

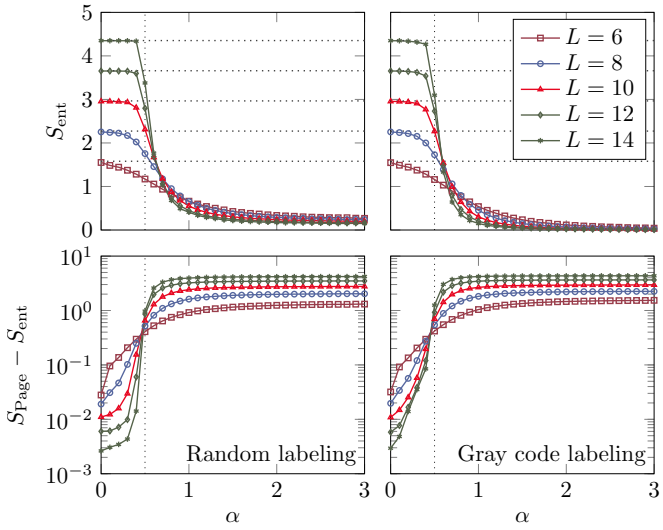

FIG. 6. Similar as Fig. 5, but now for the eigenstates corresponding to the eigenvalues with the highest and lowest energies (that is, the ground state and the antiground state). Here, the vertical dotted lines mark $\alpha = 1/2$.

B. Spectral edge eigenstates

Fig. 6 shows the same plots as discussed above, but now for the spectral-edge eigenstates. The crossing separating regimes with volume-law and area-law scaling of $S_{\rm ent}$ is now located at $\alpha \approx 1/2$. (In contrast to $\alpha \approx 1$ seen in Fig. 5 for the bulk eigenstates.) In the following sections, we study the transition points, as well as how the transition point moves across the spectrum as a function of α.

V. FINITE-SIZE DEPENDENCE

In Figures 5 and 6, we saw crossings near $\alpha \approx 1$ and near $\alpha \approx 1/2$ for the bulk and edge eigenstates, respectively. In this section, we present a finite size scaling analysis to determine the value α_0 of the power-law exponent α at which the scaling of the entanglement entropy changes from volume-law to area-law in the thermodynamic limit. Based on the theory discussed above, and on the data in Figs. 5 and 6, we expect $\alpha_0 = 1$ for the bulk and $\alpha_0 = 1/2$ for the spectral-edge eigenstates.

The quantity α_0 can be estimated from the numerical data through various finite-size scaling procedures. We have performed several scaling analyses, leading to consistent results. Here we present one such analysis. We quantify the value α_0 as the point where

$$S_{\rm ent} = S_{\rm Page} - \gamma, \tag{9}$$

after ensemble-averaging, for some reasonable value of γ. We will investigate this for several values of $\gamma > 0$. Figs. 5 and 6 show that this point can be found for all system sizes roughly over the range $\gamma \in [0.05, 0.5]$. Empirically, we find that plotting the corresponding values as a function of $1/L^2$ allows for an extrapolation towards the thermodynamic limit in all settings that we consider.

Fig. 7 shows the values of α at which condition (9) holds as a function of $1/L^2$ for both the spectral bulk (left panels) and edge (right panels) eigenstates for $\gamma = 0.05$ (top panels) and $\gamma = 0.5$ (middle panels). The connecting lines are least-square fits of the second-order polynomial

$$\alpha = \alpha_0 + \alpha_1(1/L^2) + \alpha_2(1/L^2)^2 \tag{10}$$

with (least-squares) fitting parameters α_0, α_1, and α_2. We observe that these fitted lines connect all data points reasonably well, although the fitting quality is better for the bulk than for the edge. We focus on generic values of $\gamma \in [0.05, 0.5]$ in the bottom panels, which show the estimated transition point α_0 as a function of γ together with their uncertainty (95% confidence interval of the fit (10)). The estimates of α_0 for the binary and Gray code labeling schemes are near their expected values over the full range. We observe a significant deviation for the random labeling scheme. Importantly, this means that the entanglement properties of the power-law banded random matrix ensemble interpreted as Hamiltonians of quantum many-body systems depend on the choice of the labeling scheme. For small values of γ, the condition is met for values of α below the crossing, leading to a flow towards

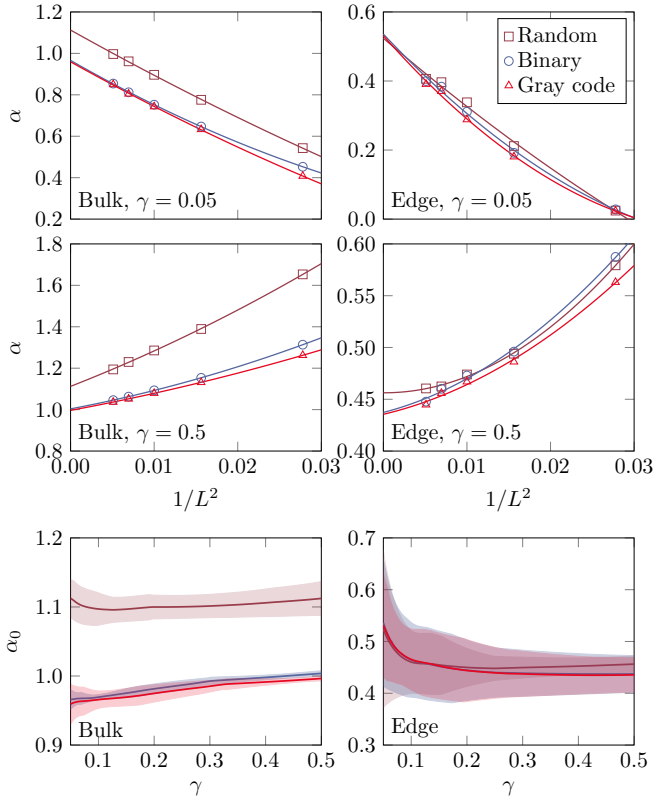

FIG. 7. The values of α for which $S_{\text{Page}} - S_{\text{ent}} = \gamma$ as a function of $1/L^2$ (after ensemble-averaging). The squares, circles, and triangles denote data for the random, binary, and Gray code labeling scheme, respectively. The spectral bulk (left column) and edge (right column) eigenstates are the same as the ones considered in Figs. 5 and 6, respectively. The solid lines give least-square fits of the form (10). The lower panels show the extrapolated value α_0 for $L \to \infty$ as a function of γ. The shaded regions in the lower panels indicate the 95% confidence interval of the fit (10).

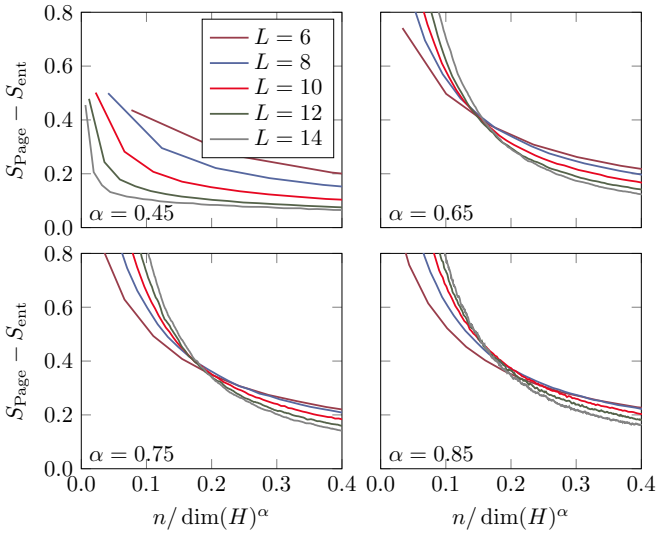

FIG. 8. The difference between the ensemble-averaged eigenstate entanglement entropy and the Page value for the Gray code labeling scheme as a function of the eigenstate index n (starting from $n = 1$ and ordered by increasing energy), scaled by $\dim(H)^\alpha$.

larger values with increasing system size. The opposite occurs for large values of γ.

VI. BOUNDARY BETWEEN BULK AND EDGE

A natural follow-up question is how the transitions at $\alpha \approx 1/2$ for the edge and $\alpha \approx 1$ for the bulk eigenstates are related to each other. In the regime $\alpha \in (1/2, 1)$, the bulk eigenstates show volume law entanglement, while the edge eigenstates show area-law entanglement. The bulk eigenstates form a measure one fraction of all eigenstates, while the number of edge eigenstates is subextensive. We thus expect that normalizing the eigenstate index n by $[\dim(H)]^\delta$, where δ is a nontrivial exponent, should show a crossing at $S_{\text{Page}} - S_{\text{ent}}$.

In Fig. 8, we find surprisingly good results for $\delta = \alpha$, where we adapt the Gray code labeling scheme. Remarkably, for fixed α within the weakly ergodic phase (that is, $\alpha \in (1/2, 1)$), we see the curves for the different system sizes to cross at fixed $n/\dim(H)^\alpha \approx 0.2$. Below (above) this point, we see a decreasing (increasing) value of the eigenstate entanglement entropy with increasing system size. The nontrivial exponent δ is thus (at least approximately) given by $\delta = \alpha$. At present we are not aware of an analytic derivation of this result.

Fig. 9 elaborates further on this by showing the ensemble-averaged eigenstate entanglement entropy for the eigenstates with the lowest and highest $0.2N^\alpha$ energies as a function of α for several system sizes. The quantity $S_{\text{Page}} - S_{\text{ent}}$ (left panel) shows a crossing at $\alpha \approx 0.5$, while $S_{\text{ent}}/S_{\text{Page}}$ (right panel) shows a crossing at $\alpha \approx 1$. This implies that the $\approx 0.2N^\alpha$ states at the spectral edges have $\mathcal{O}(1)$ deviation from S_{Page} for $1/2 < \alpha < 1$, but the majority of these states still have volume-law scaling.

Note that, contrary to what one might naively expect from Fig. 6, the finite deviation of S_{ent} from S_{Page} at $\alpha \to 1/2 + 0^+$ happens not for a finite number ($\sim N^0$) of spectral edge eigenstates, but for a number $\sim N^{1/2}$ of eigenstates that grows with N. This behavior can be understood via the fact that the transition from the weakly to the fully ergodic phase at $\alpha = 1/2$ happens in terms of the entanglement deviation from the Page value going to zero, but not in terms of the shrinking number of area-law spectral edge eigenstates going to zero. This type of the transition is similar to the quantum Zeno one where the fractal dimension, the analogue of our critical exponent δ, does not undergo any transition, while the prefactor (the analogue of our $S_{\text{Page}} - S_{\text{ent}}$) develops a jump at the transition from a finite to zero value [74].

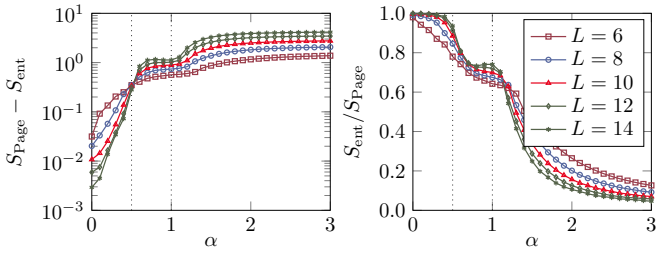

FIG. 9. The difference between the ensemble-averaged eigenstate entanglement entropy and the Page value (left panel), and the ensemble-averaged eigenstate entanglement entropy divided by the Page value as a function (right panel) of α for the Gray code labeling scheme. Here, the eigenstates with the highest and lowest $\lceil 0.2N^{\alpha} \rceil$ energies are analyzed. The vertical dotted lines mark $\alpha = 1/2$ and $\alpha = 1$.

VII. CONCLUSIONS AND OUTLOOK

In this work we explored interpretations of the power-law banded random matrix ensemble as Hamiltonians of one-dimensional quantum many-body systems, either disordered or chaotic. This was motivated by the observation that this class of random matrices, in the weakly ergodic region, displays the distinction between edge and bulk eigenstates that is typical of many-body quantum systems, namely, the edge eigenstates have area-law entanglement and the bulk eigenstates have volume-law entanglement. In addition, we expect this work to be of interest for studies on ergodicity breaking in disordered interacting quantum many-body systems.

We proposed and compared three different ways to assign many-body product basis states to the basis vectors of the random matrices. We argued our Gray code labeling scheme to improve on the previously proposed binary labeling scheme, and pointed out the need to apply what we referred to as "site randomization". We numerically studied the physical properties of the resulting Hamiltonians. We investigated the dependence of the bipartite eigenstate entanglement entropy in each of the phases, and for all the labeling schemes. We found different transition points between area-law and volume-law scaling for the eigenstates associated with the bulk and the edge of the energy spectra. Finally, we empirically found a finite-size scaling that describes the boundary between area-law and volume-law entangled eigenstates as a function of the power-law exponent.

We close with a number of suggestions for further investigations. Quantum many-body systems are typically characterized by interactions that are (spatially) local in nature. A significant improvement in interpreting random matrix ensemble as Hamiltonians of disordered quantum many-body systems could be made by finding a labeling scheme that adapts for the locality of interactions. Another obvious open question is concerned with the finite-size scaling depicted in Fig. 8 and the entanglement scaling depicted in Fig. 9, which currently have essentially the status of an empirical observation. We expect it to be a fruitful endeavor to incorporate this in the theoretical understanding of power-law banded random matrices. More straightforwardly, our findings could be extended to different types of random matrices, for example to model open or driven quantum many-body systems.

ACKNOWLEDGMENTS

MH acknowledges support from the Deutsche Forschungsgemeinschaft under grant SFB 1143 (project-id 247310070). IMK acknowledges support by the European Research Council under the European Union's Seventh Framework Program Synergy ERC-2018-SyG HERO-810451.

[1] T. Vojta, Disorder in quantum many-body systems, Ann. Rev. Condens. Matter Phys. **10**, 233 (2019).
[2] D. A. Abanin, E. Altman, I. Bloch, and M. Serbyn, Colloquium: Many-body localization, thermalization, and entanglement, Rev. Mod. Phys. **91**, 021001 (2019).
[3] P. Sierant, M. Lewenstein, A. Scardicchio, L. Vidmar, and J. Zakrzewski, Many-body localization in the age of classical computing, Rep. Prog. Phys. **88**, 026502 (2024).
[4] A. Gyenis, A. Di Paolo, J. Koch, A. Blais, A. A. Houck, and D. I. Schuster, Moving beyond the transmon: Noise-protected superconducting quantum circuits, PRX Quantum **2**, 030101 (2021).
[5] C. Berke, E. Varvelis, S. Trebst, A. Altland, and D. P. DiVincenzo, Transmon platform for quantum computing challenged by chaotic fluctuations, Nat. Comm **13**, 2495 (2022).
[6] S.-D. Börner, C. Berke, D. P. DiVincenzo, S. Trebst, and A. Altland, Classical chaos in quantum computers, Phys. Rev. Res. **6**, 033128 (2024).
[7] M. L. Mehta, *Random Matrices*, 2nd ed. (Academic Press, London, 1991).
[8] T. Guhr, A. Müller-Groeling, and H. A. Weidemüller, Random-matrix theories in quantum physics: Common concepts, Phys. Rep. **299**, 189 (1998).
[9] F. Haake, *Quantum Signatures of Chaos* (Springer-Verlag, Berlin, 2010).
[10] J. M. Deutsch, Quantum statistical mechanics in a closed system, Phys. Rev. A **43**, 2046 (1991).
[11] M. Srednicki, Chaos and quantum thermalization, Phys. Rev. E **50**, 888 (1994).
[12] M. Rigol and L. F. Santos, Quantum chaos and thermalization in gapped systems, Phys. Rev. A **82**, 011604 (2010).
[13] P. Reimann, Generalization of von Neumann's approach to thermalization, Phys. Rev. Lett. **115**, 010403 (2015).

[14] L. D'Alessio, Y. Kafri, A. Polkovnikov, and M. Rigol, From quantum chaos and eigenstate thermalization to statistical mechanics and thermodynamics, Adv. Phys. **65**, 239 (2016).

[15] F. Borgonovi, F. M. Izrailev, L. F. Santos, and V. G. Zelevinsky, Quantum chaos and thermalization in isolated systems of interacting particles, Phys. Rep. **626**, 1 (2016).

[16] C. Gogolin and J. Eisert, Equilibration, thermalisation, and the emergence of statistical mechanics in closed quantum systems, Reports on Progress in Physics **79**, 056001 (2016).

[17] R. Mondaini and M. Rigol, Eigenstate thermalization in the two-dimensional transverse field Ising model. II. Off-diagonal matrix elements of observables, Phys. Rev. E **96**, 012157 (2017).

[18] J. M. Deutsch, Eigenstate thermalization hypothesis, Reports on Progress in Physics **81**, 082001 (2018).

[19] I. M. Khaymovich, M. Haque, and P. A. McClarty, Eigenstate thermalization, random matrix theory, and behemoths, Phys. Rev. Lett. **122**, 070601 (2019).

[20] S. Sugimoto, R. Hamazaki, and M. Ueda, Test of the eigenstate thermalization hypothesis based on local random matrix theory, Phys. Rev. Lett. **126**, 120602 (2021).

[21] N. Rosenzweig and C. E. Porter, "Repulsion of energy levels" in complex atomic spectra, Phys. Rev. **120**, 1698 (1960).

[22] V. E. Kravtsov, I. M. Khaymovich, E. Cuevas, and M. Amini, A random matrix model with localization and ergodic transitions, New J. Phys. **17**, 122002 (2015).

[23] D. Facoetti, P. Vivo, and G. Biroli, From non-ergodic eigenvectors to local resolvent statistics and back: A random matrix perspective, Europhys. Lett. **115**, 47003 (2016).

[24] K. Truong and A. Ossipov, Eigenvectors under a generic perturbation: Non-perturbative results from the random matrix approach, Europhys. Lett. **116**, 37002 (2016).

[25] M. Amini, Spread of wave packets in disordered hierarchical lattices, Europhys. Lett. **117**, 30003 (2017).

[26] P. von Soosten and S. Warzel, Non-ergodic delocalization in the Rosenzweig–Porter model, Lett. Math. Phys. **109**, 1 (2018).

[27] C. Monthus, Multifractality of eigenstates in the delocalized non-ergodic phase of some random matrix models: Wigner-Weisskopf approach, J. Phys. A: Math. Theor. **50**, 295101 (2017).

[28] V. E. Kravtsov, I. M. Khaymovich, B. L. Altshuler, and L. B. Ioffe, Localization transition on the random regular graph as an unstable tricritical point in a log-normal Rosenzweig-Porter random matrix ensemble, arXiv:2002.02979 (2020).

[29] I. M. Khaymovich, V. E. Kravtsov, B. L. Altshuler, and L. B. Ioffe, Fragile extended phases in the log-normal Rosenzweig-Porter model, Phys. Rev. Res. **2**, 043346 (2020).

[30] G. Biroli and M. Tarzia, Lévy-Rosenzweig-Porter random matrix ensemble, Phys. Rev. B **103**, 104205 (2021).

[31] I. M. Khaymovich and V. E. Kravtsov, Dynamical phases in a "multifractal" Rosenzweig-Porter model, SciPost Phys. **11**, 045 (2021).

[32] W. Buijsman and Y. Bar Lev, Circular Rosenzweig-Porter random matrix ensemble, SciPost Phys. **12**, 082 (2022).

[33] G. De Tomasi and I. M. Khaymovich, Non-Hermitian Rosenzweig-Porter random-matrix ensemble: Obstruction to the fractal phase, Phys. Rev. B **106**, 094204 (2022).

[34] D. Venturelli, L. F. Cugliandolo, G. Schehr, and M. Tarzia, Replica approach to the generalized Rosenzweig-Porter model, SciPost Phys. **14**, 110 (2023).

[35] M. Sarkar, R. Ghosh, and I. M. Khaymovich, Tuning the phase diagram of a Rosenzweig-Porter model with fractal disorder, Phys. Rev. B **108**, L060203 (2023).

[36] R. Ghosh, M. Sarkar, and I. M. Khaymovich, Inverse kinetic effects: Localization and re-entrant transitions, arXiv:2411.16851 (2024).

[37] A. Kutlin and I. M. Khaymovich, Anatomy of the eigenstates distribution: A quest for a genuine multifractality, SciPost Phys. **16**, 008 (2024).

[38] Y. V. Fyodorov, A. Ossipov, and A. Rodriguez, The Anderson localization transition and eigenfunction multifractality in an ensemble of ultrametric random matrices, J. Stat. Mech.: Theory Exp. **2009**, L12001.

[39] E. Bogomolny and O. Giraud, Eigenfunction entropy and spectral compressibility for critical random matrix ensembles, Phys. Rev. Lett. **106**, 044101 (2011).

[40] I. Rushkin, A. Ossipov, and Y. V. Fyodorov, Universal and non-universal features of the multifractality exponents of critical wavefunctions, J. Stat. Mech.: Theory Exp. **2011**, L03001.

[41] B. Gutkin and V. A. Osipov, Spectral problem of block-rectangular hierarchical matrices, J. Stat. Phys. **143**, 72 (2011).

[42] J. A. Méndez-Bermúdez, A. Alcázar-López, and I. Varga, Multifractal dimensions for critical random matrix ensembles, Europhys. Lett. **98**, 37006 (2012).

[43] P. von Soosten and S. Warzel, The phase transition in the ultrametric ensemble and local stability of Dyson Brownian motion, Electron. J. Probab. **23**, 1 (2018).

[44] E. Bogomolny and M. Sieber, Power-law random banded matrices and ultrametric matrices: Eigenvector distribution in the intermediate regime, Phys. Rev. E **98**, 042116 (2018).

[45] P. von Soosten and S. Warzel, Delocalization and continuous spectrum for ultrametric random operators, Ann. Henri Poincaré **20**, 2877 (2019).

[46] J. Šuntajs, M. Hopjan, W. De Roeck, and L. Vidmar, Similarity between a many-body quantum avalanche model and the ultrametric random matrix model, Phys. Rev. Res. **6**, 023030 (2024).

[47] A. D. Mirlin, Y. V. Fyodorov, F.-M. Dittes, J. Quezada, and T. H. Seligman, Transition from localized to extended eigenstates in the ensemble of power-law random banded matrices, Phys. Rev. E **54**, 3221 (1996).

[48] V. E. Kravtsov and K. A. Muttalib, New class of random matrix ensembles with multifractal eigenvectors, Phys. Rev. Lett. **79**, 1913 (1997).

[49] I. Varga and D. Braun, Critical statistics in a power-law random-banded matrix ensemble, Phys. Rev. B **61**, R11859 (2000).

[50] A. D. Mirlin and F. Evers, Multifractality and critical fluctuations at the Anderson transition, Phys. Rev. B **62**, 7920 (2000).

[51] E. Cuevas and V. E. Kravtsov, Two-eigenfunction correlation in a multifractal metal and insulator, Phys. Rev. B **76**, 235119 (2007).

[52] F. Evers and A. D. Mirlin, Anderson transitions, Rev. Mod. Phys. **80**, 1355 (2008).

[53] G. De Tomasi, Algebraic many-body localization and its implications on information propagation, Phys. Rev. B **99**, 054204 (2019).

[54] P. A. Nosov, I. M. Khaymovich, and V. E. Kravtsov, Correlation-induced localization, Phys. Rev. B **99**, 104203 (2019).

[55] D. A. Vega-Oliveros, J. A. Méndez-Bermúdez, and F. A. Rodrigues, Multifractality in random networks with power-law decaying bond strengths, Phys. Rev. E **99**, 042303 (2019).

[56] M. Haque, P. A. McClarty, and I. M. Khaymovich, Entanglement of midspectrum eigenstates of chaotic many-body systems: Reasons for deviation from random ensembles, Phys. Rev. E **105**, 014109 (2022).

[57] A. D. Mirlin, Statistics of energy levels and eigenfunctions in disordered systems, Phys. Rep. **6326**, 259 (2000).

[58] F. Evers and A. D. Mirlin, Fluctuations of the inverse participation ratio at the Anderson transition, Phys. Rev. Lett. **84**, 3690 (2000).

[59] V. L. Quito, P. Titum, D. Pekker, and G. Refael, Localization transition in one dimension using Wegner flow equations, Phys. Rev. B **94**, 104202 (2016).

[60] G. De Tomasi and I. M. Khaymovich, Non-Hermiticity induces localization: Good and bad resonances in power-law random banded matrices, Phys. Rev. B **108**, L180202 (2023).

[61] S. Ghosh, M. Kulkarni, and S. Roy, Eigenvector correlations across the localization transition in non-Hermitian power-law banded random matrices, Phys. Rev. B **108**, L060201 (2023).

[62] I. Vallejo-Fabila, A. K. Das, D. A. Zarate-Herrada, A. S. Matsoukas-Roubeas, E. J. Torres-Herrera, and L. F. Santos, Reducing dynamical fluctuations and enforcing self-averaging by opening many-body quantum systems, Phys. Rev. B **110**, 075138 (2024).

[63] V. Tiwari, D. S. Bhakuni, and A. Sharma, Periodically and aperiodically Thue-Morse driven long-range systems: From dynamical localization to slow dynamics, arXiv:2412.19736 (2024).

[64] Y. Y. Atas and E. Bogomolny, Multifractality of eigenfunctions in spin chains, Phys. Rev. E **86**, 021104 (2012).

[65] W.-J. Rao, Power-law random banded matrix ensemble as the effective model for many-body localization transition, Eur. Phys. J. Plus **137**, 398 (2022).

[66] A. Bäcker, M. Haque, and I. M. Khaymovich, Multifractal dimensions for random matrices, chaotic quantum maps, and many-body systems, Phys. Rev. E **100**, 032117 (2019).

[67] L. S. Levitov, Absence of localization of vibrational modes due to dipole-dipole interaction, Europhys. Lett. **9**, 83 (1989).

[68] L. S. Levitov, Delocalization of vibrational modes caused by electric dipole interaction, Phys. Rev. Lett. **64**, 547 (1990).

[69] E. Bogomolny and M. Sieber, Eigenfunction distribution for the Rosenzweig-Porter model, Phys. Rev. E **98**, 032139 (2018).

[70] F. Gray, Pulse code communication, U.S. Patent 2,632,058 (1953).

[71] R. W. Doran, The Gray code, Journal of Universal Computer Science **13**, 1573 (2007).

[72] E. Lubkin, Entropy of an n-system from its correlation with a k-reservoir, J. Math. Phys. **19**, 1028 (1978).

[73] D. N. Page, Average entropy of a subsystem, Phys. Rev. Lett. **71**, 1291 (1993).

[74] P. Sierant and X. Turkeshi, Universal behavior beyond multifractality of wave functions at measurement-induced phase transitions, Phys. Rev. Lett. **128**, 130605 (2022).